J.J. Mendoza Lopetegui, G. Papa, M. Morandini, M. Tanelli
Data-Driven Modeling and Regulation of Aircraft Brakes Degradation via Antiskid Controllers
IEEE Transactions on Reliability, Published online 10/08/2022
doi:10.1109/TR.2022.3194646

Data-driven Modelling and Regulation of Aircraft Brakes Degradation via Anti-skid Controllers

José Joaquín Mendoza Lopetegui, Gianluca Papa, Marco Morandini, and Mara Tanelli, *Senior Member, IEEE*

***Abstract*—In ground vehicles, braking actuator degradation and tire consumption do not represent a significant maintenance cost as the lifespan of both components, at least in common situations, is rather long. In the aeronautical context, and for aircraft in particular, instead, braking actuator degradation and tire consumption significantly contribute to an aircraft maintenance cost due to the frequency of their replacement. This is mainly due to the fact that aircraft braking maneuvers last significantly longer than those in the automotive context. So that the anti-lock braking system is always active during the braking maneuver, making its impact on the consumption of the two components significant. This work proposes an innovative data-driven model of brake and tire degradation, showing how they are related to the anti-skid controller parameters. The analysis is carried out in a Matlab/Simulink environment on a single wheel rigid body model, validated experimentally, which includes all the nonlinear effects peculiar of the aeronautic context. The results show that by using an appropriate anti-skid control approach, it is possible to directly regulate the consumption of these components while at the same time guaranteeing the required braking performance.**

***Index Terms*—Aircraft, anti-skid control, wheel slip control, braking actuator wear, tire wear.**

I. Introduction

FOLLOWING the development of braking actuators technology, which now allows for a continuous adjustment of the braking torque, leading-edge anti-lock braking system (ABS) control strategies in the automotive context can nowadays be formulated as a wheel slip tracking task, see [1]–[5], with the control law being defined by solving a continuous dynamic problem. These braking control strategies not only can avoid wheel locking, which is the main purpose of an ABS, but can also achieve high braking performance. The first version of ABS algorithms were operated by switching logics based on the alternation of three discrete set of control actions, *i.e.*, HOLD, DECREASE and INCREASE due to the limited capabilities of the previous generation of braking actuators. The transitions among these discrete states were piloted by thresholds based on the controlled variable, which could be either the wheel deceleration [6]–[9], or the wheel slip [10]–[13]. These transitions were designed so as to ensure a stable limit cycle around a fixed wheel slip value, selected a-priori and kept constant for all surfaces, thus resulting in a significant sub-optimal performance. Wheel slip based approaches are more robust and performing compared to deceleration based ones. However, their use comes with the challenge of vehicle longitudinal speed estimation, which is needed to compute the slip value. Nowadays, standard vehicle speed estimation approaches make use of the four wheel speed velocities and longitudinal acceleration signals. In the literature these approaches span from fuzzy-logic [14], [15], to extended Kalman Filter and sensor fusion [16], [17], non-linear observers [18]–[20], recursive identification methods, [21] and *ad-hoc* signal processing techniques, [11].

Safety and certification issues in the aeronautical field have so far prevented the use of measurements not directly available on the landing gear, which are limited to the wheel speeds and braking pressure. Hence, current ABS approaches are still mostly deceleration-based, and they aim at generating a stable limit cycle on the wheel speeds. Recent works, see *e.g.*, [22], [23] proved that a wheel slip control approach, could provide significant advantages, not only increasing performance and reducing the time needed for design and tuning, but also allowing a direct control of the tire usage. The longitudinal speed estimation problem is particularly challenging in the aeronautic context, because of the aforementioned limitation in the available measurements. Recent results, see [24], [25], have shown that the aircraft speed can be reliably obtained without requiring changes in the current landing gear layout, paving the way for the employment of wheel slip based anti-skid control strategies also in the aeronautic field.

An important difference between the automotive and aeronautical contexts is in the frequency and duration of the anti-skid control action. In the automotive field, the ABS is rarely activated, and only for relatively short time intervals, up to few seconds. On the contrary, in the aeronautic field, the ABS is usually used in every braking maneuver, both in Landing (LND) and Rejected Take Off (RTO). These actions last from the beginning of the braking maneuver until the aircraft is in standstill, with an average time duration ten times higher than that in the automotive case. Because of the duration of the braking maneuver, the anti-skid controller has to cope with significantly time varying working conditions. These involve a large longitudinal speed decrease, a large load variation due to the ever-changing aerodynamic forces and also changes of the braking actuator performance, induced by the overheating of the actuator components, see [26]–[28]. The duration of the braking maneuver significantly impacts the braking actuator and tire consumption, the combination of which accounts for most of the landing gear maintenance costs because the total mechanical energy of the aircraft is

J. J. Mendoza Lopetegui, G. Papa, and M. Tanelli are with the Dipartimento di Elettronica, Informazione e Bioingegneria, Politecnico di Milano, 20133 Milan, Italy (e-mail: josejoaquin.mendoza@polimi.it; gianluca.papa@polimi.it; mara.tanelli@polimi.it).

M. Morandini is with the Dipartimento di Ingegneria Aerospaziale, Politecnico di Milano, via La Masa 34, 20156 Milano, Italy (e-mail: marco.morandini@polimi.it).

mostly dissipated by these two main components. Focusing on the tire, it is well known from the literature, see [29], [30], that the wear phenomenon is caused by the sliding motion between the wheel and runway surfaces, which is necessary to generate the longitudinal contact force that is required to decelerate the aircraft, with the total mass of tire consumed being proportional to the sliding distance. For the braking actuator instead, the wear phenomenon is related to the braking pad consumption. This, in turn, is caused by the sliding motion between the braking pads and wheel disc surfaces, and for this reason it is proportional to the applied pressure per unit of surface and to the sliding distance [31]. The sliding between the wheel and road surface, as well as the one between the braking pads and wheel disc, are not independent, but instead they are coupled and connected via the applied pressure, which is regulated by the anti-skid controller [22], [23]. The pressure profile commanded by the anti-skid controller for a given aircraft braking maneuver determines the distribution of the energy dissipated between the two components and hence their relative consumption. Therefore, the performance of the braking control algorithm can be directly linked to the braking actuator and tire energy consumption.

Most of the attempts that have been made in order to characterize the brake consumption dynamics focus on the local description of wear mechanisms in braking systems [26], [32], [33], often generating Finite Element (FE) models aiming to identify surface wear characteristics. However, the resultant models are difficult to use in practical situations for anti-lock braking system design, as the relationship with the anti-skid system is not clear, especially for aeronautical applications. Instead, we propose the usage of a data-driven model to capture the brake consumption dynamics, which can be directly obtained from tests carried out during conventional anti-skid system prototyping, and which captures the inherent stochastic nature of the phenomenon. A more in-depth discussion of the approach is provided in Section IV.

This paper shows how to effectively model the braking consumption dynamics and how the parameter selection for an anti-skid wheel slip-based controller can impact the relative energy absorption of the tire and braking actuator components. The analysis is carried out in a Matlab/Simulink environment, where a single wheel rigid body model for an aircraft is implemented, including non linear effects due to vertical load variation, and a high fidelity model for the braking actuator which accurately models the wear dynamic of the component over its lifespan, validated on experimental data collected in real flywheel tests. To prove the effectiveness of the overall approach, a set of different maneuvers has been defined, comprising multiple aircraft operating conditions in terms of mass, road friction and initial velocities. Further, closed loop experiments with a wheel slip based controller were performed, with varying reference value $\bar{\lambda}$, evaluating tire and braking actuator energy consumption over the different maneuvers for each controller configuration. The results show that, by properly selecting the reference wheel slip value, it is possible to control the tire and braking actuator usage while maximizing the anti-skid controller performance over the defined set of maneuvers.

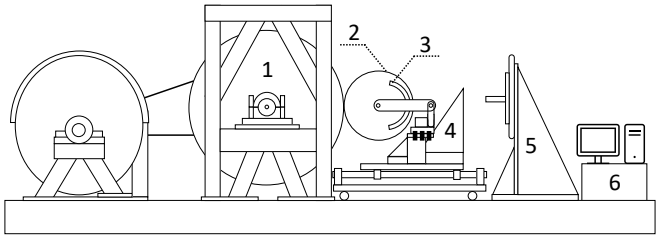

Fig. 1. Schematic representation of the experimental test rig and its main components highlighted in numbers: 1) Flywheel 2) Landing gear 3) Brake pad and disk 4) Moving sledge 5) Loading device 6) Computer-based anti-skid controller.

To the author's best knowledge, this is the first attempt to characterize the braking actuators and their degradation, dynamically starting from ABS sensors, and to propose a control strategy to actively regulate it while safely braking.

The structure of the paper is as follows: Section II introduces the single landing gear experimental test rig, its main components, and the experimental procedure for the realization of a braking maneuver. Then, Section III introduces the mathematical model of the landing gear dynamics and that of the braking actuator, which together define the simulation framework used to replicate the dynamics of the experimental hardware. Section IV presents the data-driven modelling of the braking actuator degradation, including both its dynamic characteristics as well as its quasi-static decay, showing the consistency with experimental data. Section V illustrates the defined wheel slip anti-skid control, its tuning procedure and its performance on a single maneuver. Finally, Section VI presents the sensitivity analysis over a wide range of maneuvers in different operating conditions, highlighting the impact of the selected wheel slip reference value $\bar{\lambda}$ on the tire and braking actuator energy consumption, showing how these quantities can be directly controlled by the proposed framework.

II. Experimental setup and simulation setting

The design and preliminary testing phases of an anti-skid controller in the aeronautic context is usually carried out using hardware in the loop test rigs. The one used in this work focuses on the Main Landing Gear, and consists of six main components: the flywheel simulating the road surface; a moving sledge; a loading device used to simulate the touchdown with a prescribed vertical load acting on the tire; the real Main Landing Gear assembly that includes the wheel and its structural mechanical elements; the braking actuator; and an anti-skid controller operated by a dedicated computer. The schematic representation of the test rig along with its main components is provided in Fig. 1. An experimental braking maneuver performed using this test rig can be decomposed into three consecutive phases. During the first phase, the flywheel is not in contact with the landing gear, and its velocity is increased up to a prescribed reference value, which depends on the selected mass condition. The second phase simulates the touch down phenomenon, by pushing the sliding edge with the loading device, so that the landing gear wheel is put in contact with the flywheel with a prescribed load value that

is a function of the simulated longitudinal speed. Similarly to the real scenario, the braking maneuver is started after a time interval necessary to stabilize the wheel speed oscillations induced by the touch down event. During the third and final deceleration phase, the vertical load is changed dynamically to simulate the lift variation, and consequently the wheel radius reduction due to the application of the vertical load. The braking pressure is applied to the landing gear with the real actuator, *i.e.* a proportional pressure valve controlled in current, which allows for continuous pressure modulation. The experimental test rig can be used in both open and closed loop configurations of the aircraft, with the only difference between the two being the shape of the current profile which is either specified automatically by the anti-skid controller or manually by the driver/pilot. The main purpose of the introduced experimental set up is the implementation and testing of advanced anti-skid control strategies, see [34] for further details.

In this work, we implement a combination of a model-based simulation environment and a data-driven model that is able to replicate the dynamics of the described experimental hardware. In Section III, the description of the model-based simulation environment is presented, together with validation results using experimental data collected from closed loop tests carried out on the rig. In Section IV, the data-driven model of the braking actuator degradation is presented, which enables to augment the model-based simulation from Section III.

III. Landing gear modelling

Several models exist in the literature that are capable of capturing different aspects of landing gear dynamics. An overview of different approaches can be consulted in [35] and references therein, which remark the suitability of multibody simulation environments for aeronautic applications due to the complexity level often encountered. The landing gear may be represented in its entirety, or its parts may be considered separately, depending on the aircraft topology. Specific models have been devised to study certain phenomena in particular operating conditions, such as gear-walk [36], shimmy [37], or response to component failure [38]. For the application at hand, the chosen modelling framework needs to be instrumental for anti-skid control system design, be able to replicate the dynamics of the experimental test rig described in Section II, and be as simple as possible to clearly link the braking actuator degradation to the anti-skid design parameters. Given the previous considerations, the simulation environment used within this work of research consists of a rigid body representation of the experimental test rig described in Section II, which corresponds to a single-wheel model of the Main Landing Gear (MLG). This choice is consistent with an aircraft with tricycle landing gear configuration with an MLG equipped with anti-skid capabilities. The model considers vertical load variation, radius variation, friction curve characteristic shape, and actuator static behavior identified from experimental tests performed with the test rig.

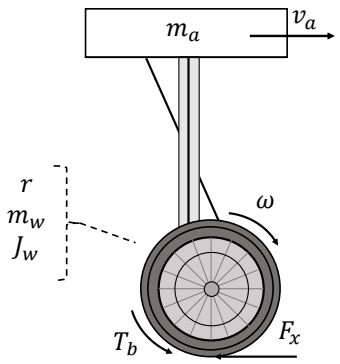

Fig. 2. Conceptual representation of an aircraft landing gear single-wheel model and its main variables.

A. Landing gear dynamic model

Fig. 2 provides a graphical representation of the longitudinal and wheel rotational dynamics implemented via the experimental test rig. With reference to Fig. 2, the landing gear dynamic model is given by the following set of equations:

$$m_a \dot{v}_a = -F_x \tag{1a}$$

$$\dot{\omega} J_w = r F_x - T_b \tag{1b}$$

where

$$F_x = F_z \mu(\lambda),\ F_z = F_z(v_a),\ r = r(F_z),\ T_b = k_b P_b$$

with F_x and F_z being the longitudinal and vertical force acting on the wheel, while T_b and P_b representing the braking torque, and pressure. The first equation (1a) describes the longitudinal aircraft dynamics and includes the inertial term $m_a \dot{v}_a$ and the tire contact force F_x, positive during braking and computed as the product between the vertical load $F_z(v_a)$, function of the longitudinal velocity v_a, so that:

$$F_z(v_a) = m_a g - \frac{1}{2} \rho v_a^2 S C_l \tag{2}$$

with m_a being the total mass of the aircraft acting on the wheel, and $\frac{1}{2}\rho v_a^2 S C_l$ the lifting component of the aerodynamic force, and the friction coefficient $\mu(\lambda)$, which is a function of the longitudinal wheel slip λ defined as:

$$\lambda = \frac{v_a - \omega r}{v_a} \tag{3}$$

where v_a is the aircraft velocity and r is the wheel radius, function of the vertical load F_z. As for the friction model, within this simulation environment the Burckhardt model was selected, see [11]. Based on this model, the longitudinal friction coefficient $\mu(\lambda)$ has the following form:

$$\mu(\lambda) = c_1 (1 - e^{-c_2 \lambda}) - c_3 \lambda \tag{4}$$

where the value of the adimensional parameters c_1, c_2 and c_3 can be properly selected to describe different friction conditions. Within this simulation environment, the value of the three coefficients has been identified from experimental tests on the rig for the dry case scenario, and then modified by defining 8 different combinations, spanning from dry asphalt to ice friction conditions, see Fig. 3.

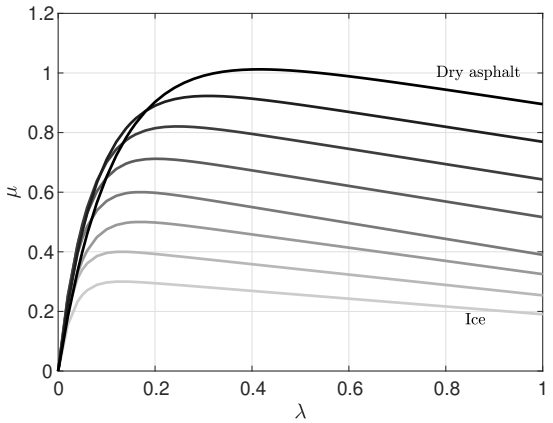

Fig. 3. Burckhardt friction model as a function of the wheel slip. The eight represented curves allow to alternate between wet/slippery surfaces (bottom curves) and dry/high-grip surfaces (top curves).

B. Braking actuator modelling

Equation (1b) describes the wheel rotational dynamics, where T_b represents the braking torque, computed as the product between the braking pressure P_b and a converting factor k_b, function of the braking actuator characteristics, the expression of which is given by:

$$k_b = \mu_b A_p N_p N_s R_{eff} \tag{5}$$

with μ_b being the braking friction coefficient, A_p the piston surface area, N_p the number of pistons, N_s the number of contact surfaces of the disc brake and R_{eff} the effective radius of the contact point of the sliding surfaces. The model for the proportional valve consists of both static and dynamic components, the characteristics of which have been identified experimentally on the hardware in the loop set up described in Section II. The static current/pressure relationship has been identified *via* quasi-static tests, *i.e.* slow current ramps fed as input to the actuator, and modelled in the simulation environment as a static map. The dynamic component instead has been defined from frequency sweep and step current input tests and by fitting a second order parametric transfer function. The overall actuator dynamics can be described as:

$$A(s) = k_b \frac{K_{st} e^{-\tau s}}{\left(1 + \frac{2\xi s}{\omega_n} + \frac{s^2}{\omega_n^2}\right)} \tag{6}$$

with $A(s)$ being the transfer function between the current, and obtained torque, k_b is the conversion coefficient as in Equation (5), τ is the actuator delay due to the fluid transfer, ξ is the damping coefficient, ω_n is the natural frequency and K_{st} is the varying actuator gain described by the aforementioned static map. For further details, the reader may refer to [34]. With reference to Fig. 2 and Equations (1a) and (1b) the physical meaning of the geometric and inertial parameters are provided in Table I.

C. Simulation framework validation

The complete model that simulates the dynamic of the experimental set up is implemented in Matlab/Simulink and its schematic representation presented in Fig. 4. The model is initialized with a reference mass, friction condition and longitudinal speed value, and receives as input the controlled current I_{ref}, computed either in open or closed loop. The defined simulation environment has been validated against the experimental data collected on the test rig by feeding the measured braking pressure in feed-forward, and comparing the resulting wheel and longitudinal aircraft speed.

Specifically, Fig. 5 shows the comparison between the aircraft speed obtained on the test rig v_a (dark grey), retrieved from a closed loop maneuver where the pressure profile is defined by the anti-skid controller to track a reference wheel slip value, against the one obtained from the simulation $\hat{v}_a$ (light grey), the speed estimation errors are also detailed. The maneuver in question exhibits the characteristics that can be found in a Rejected Take Off condition, in which the take off is aborted while the aircraft is still in the acceleration phase due to possible technical problems. Therefore, reduced speeds with respect to a conventional landing can be expected. In particular, the maneuver detailed in Fig. 5 has a starting speed of around 60 [km/h]. As highlighted in the top plot in Fig. 5, the longitudinal aircraft and wheel speed profiles obtained from the simulation precisely match the experimental ones. This match can be further appreciated when comparing the wheel slip profiles. In fact, considering the bottom plot in Fig. 5, it is possible to see that the wheel slip profile obtained from the simulation replicates the experimental one in both transient and static phase. The increase in the speed error prediction,

TABLE I
PARAMETERS OF THE MODEL OF THE LANDING GEAR DYNAMICS

Symbol	Meaning	Unit
J_w	wheel rotational inertia	$kg\ m^2$
r	nominal wheel radius	m
m_a	aircraft mass	kg
ρ	mass density of the fluid	kg/m^3
k_b	pressure to torque gain	m^3
S	reference surface	m^2
C_l	lifting coefficient	-

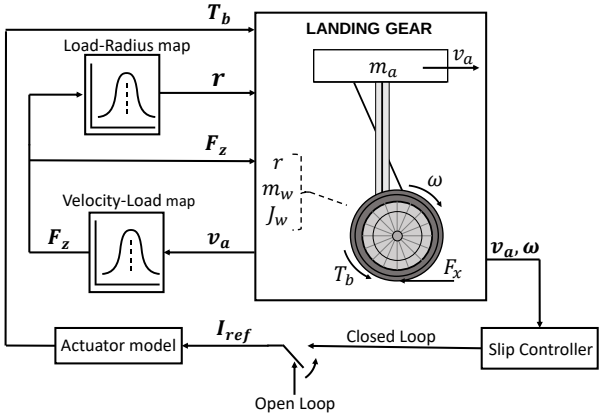

Fig. 4. Schematic representation of the single-wheel landing gear simulator, including the servo-hydraulic actuator model and nonlinear maps for the computation of the wheel radius compression and vertical load.

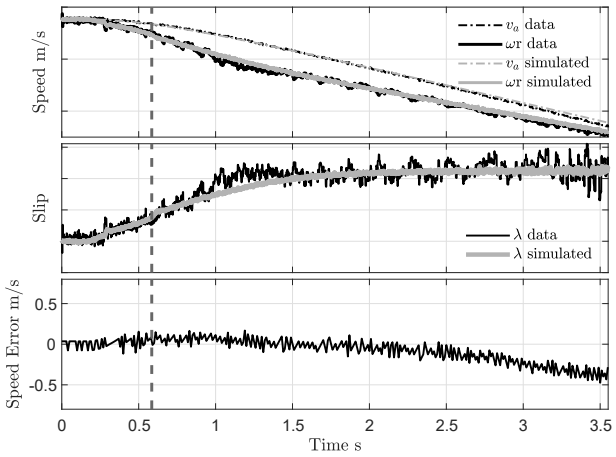

Fig. 5. Closed loop validation test of the simulated model, (black: measured data, grey: simulated data). Top plot and middle plot: Comparison between the measured and simulated wheel speed, body speed and wheel slip. Bottom plot: velocity estimation error. The vertical dotted line indicates the instant when the controller engages.

as well as the more oscillatory nature of the experimental slip values that can be observed towards the end of the braking maneuver, can be attributed to the limitations of the employed landing gear wheel and flywheel speed encoders in achieving high quality measurements in the low speed regimes.

The result from the validation shows that the defined model is capable of reproducing with high accuracy the experimental traces, confirming its possible employment as a reliable simulation means, for the analysis of the interplay between the actuator health condition and the anti-skid controller performance.

IV. Modelling of the brake degradation

In the aeronautical context, and for aircraft in particular, a significant part of the maintenance costs are shared by braking actuator and tires components, which due to the long duration of the braking maneuver, must be frequently replaced to guarantee the required braking performance. The main cause for the consumption and consequent change in performance of both components is the sliding motion between the involved surfaces: tire-road and braking pad-wheel disc, respectively. This sliding motion is necessary during the braking maneuver to transfer the required longitudinal force to the ground, which decelerates the aircraft and dissipates its mechanical energy. The performance variation in these two components must be compensated by the anti-skid controller, which is required to operate with elevated efficiency. Focusing on the brake, performance variation corresponds to changes in the braking friction coefficient value μ_b, see Equation (5), which acts as a scaling factor in the pressure to torque conversion, and can significantly vary during the actuator lifespan. This section introduces the models that have been devised to track the brake degradation, *i.e.* changes in the scaling factor μ_b which will complete the simulation framework described in Section (III), and will serve as a starting point for the result of the sensitivity analysis presented in Section VI. The value of the friction coefficient μ_b is not constant in the brake life and varies following two different dynamics. Specifically, it varies dynamically during the single braking application, and quasi-statically with respect to the actuator lifespan. Some authors have attempted to model the friction coefficient variation as a dynamical system dependent on internal variables of the braking device. One of the best known models is the Ostermeyer model, which characterizes this variation as an equilibrium of flows of growing and destroying contact patches [39]. Improvements upon this approach have been recently presented in the ILVO model [40]. More commonly, the variability of the braking coefficient is characterized for single braking maneuvers through regression-based approaches on experimental data, relying on variables such as the braking speed [26], [27] or the applied pressure [28]. In this manner, the dynamic variation of the braking coefficient during a braking maneuver is coupled with a quasi-static decay while the disc material gets worn down. The most widely used modelling approach to capture this last effect is due to Archard, where the wear is described as proportional to the load and the sliding distance [31]. Several works have subsequently appeared that use Archard's model or a slight variation of it, depending on the application at hand [32], [33], [41]. In this work, an innovative approach which takes into account also the stochastic nature of the wear dynamic is proposed, with the advantage that it can be directly extracted from conventional tests carried out during anti-skid system design and testing. In particular, this stochastic characteristic is introduced with a four-component Gaussian Mixture Model, able to capture both the trend and the stochastic nature of the observed available data from an endurance campaign in an actuator operated from brand new conditions up to failure.

TABLE II
Braking Maneuver Data

CONFIG	**mass** kg	**init. speed** m/s
Light landing	2800	49
Medium landing (a)	3150	52
Medium landing (b)	3300	53
Heavy landing	4450	61

A. Dynamic variation

A typical approach used to capture the nonlinearity of the considered actuator is to propose a proxy variable that correlates with the variation in μ_b, see [26], [27]. In this work, we must make use of a variable that is available in the ABS system, and we thus propose to use the braking speed to capture the nonlinearity of interest. The characterization of the relationship of the dynamic friction coefficient against speed was carried out in four different speed regimes, consistent with standardized braking maneuvers for the application at hand, with different aircraft mass. The characteristics of the considered landing maneuvers are presented in Table II.

The measured evolution of the friction coefficient with respect to the longitudinal aircraft speed followed three different trends, each of which is presented in Table II and in Fig.

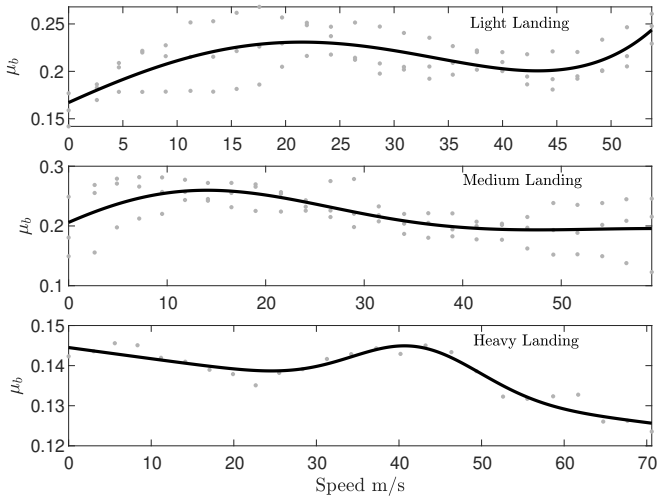

Fig. 6. Dynamic evolution of the friction coefficient during a standard maneuver. Top plot: Light Landing maneuver. Middle plot: Medium Landing maneuvers. Bottom plot: Heavy Landing maneuver. The experimental data is overlaid with the fitted curves used in the simulator for implementing the friction coefficient dynamics.

6. As can be observed, the load and brake-on speed value of the landing maneuver has a significant influence on the dynamics of the braking coefficient. In spite of this, the evolution trends could be clearly fitted for the standardized set of maneuvers defined, and the estimated regression curves used within the simulation environment to model the dynamic variation component of the braking friction μ_b.

B. Quasi-static variation

In order to further characterize the brake wear dynamics, experimental data coming from an endurance campaign performed on the braking actuator was used, employing the experimental test rig described in Section II, and represented in Fig. 1. The experimental setup requires the presence of the braking actuator being characterized, as well as a simple anti-skid controller able to follow a prescribed deceleration profile. The experimental data used in this research work consists of a set of 500 consecutive braking maneuvers, performed in the same inertial, speed, and friction configuration, see Table III. The maneuvers are carried out in closed-loop, with the braking actuator being requested to provide a pressure profile that allows it to track a prescribed wheel deceleration value. With this experimental set up, the wheel and flywheel speeds are measured using magnetic encoders, while a pressure sensor provides the measure of the braking pressure applied to the disk. Finally, the vertical load and the longitudinal force and torque are measured by load cells.

The expression of the braking friction coefficient μ_b has been retrieved by inverting equation (5), and its value was computed as

$$\overline{\mu_b} = \frac{T_{b,avg}}{P_{b,avg}} \cdot \frac{1}{A_p N_p N_s R_{eff}} \tag{7}$$

with $T_{b,avg}$ and $P_{b,avg}$ representing the measured average value of the pressure and torque signal for each braking

TABLE III
ENDURANCE TEST DATA, REPORTED WITH STANDARD DEVIATION

Variable	Value	Std. dev.	Unit
Torque	630.37	± 4.65	Nm
Load	23532.78	± 198.90	N
Speed	54.86	± 0.18	m/s
Duration	16.92	± 0.19	s
Length	464.22	± 5.46	m

maneuver, respectively. By doing so a single value of μ_b is calculated for each maneuver, and its trend mapped onto the whole endurance campaign using a suitable proxy variable. In this work, we propose to employ the cumulative energy consumed by the braking system in the 500 maneuvers. During a braking maneuver, in fact, the work W required to reduce the aircraft from an initial velocity $v_1 \neq 0$ and a rotational wheel speed $\omega_1 \neq 0$ to $v_2 \neq 0$ and $\omega_2 \neq 0$ is given by

$$W = \frac{1}{2} m (v_1^2 - v_2^2) + \frac{1}{2} J (\omega_1^2 - \omega_2^2) \tag{8}$$

Further, for a generic aircraft braking maneuver, the work W can be split into three main components

$$W = \int_{t_1}^{t_2} \Big(F_x(t)\lambda(t)v(t) + T_b(t)\omega(t) + v(t)F_a(t) \Big) dt \tag{9}$$

where F_x is the tire-runway longitudinal force, λ is the wheel slip, T_b is the braking torque and F_a is the drag force experienced by the aircraft. The first component represents the energy dissipated by the tire, the second one corresponds to the energy dissipated by the braking system, while the third one is the energy loss due to drag, which was not included in our experimental set up. Clearly, the component of interest for describing the brake degradation is the energy dissipated by the braking system, the value of which depends on the braking torque T_b and on the wheel speed ω signals, see equation (9), both measured with the employed experimental set up. Fig. 7 shows the braking coefficient $\overline{\mu_b}$ calculated for each maneuver, plotted against the cumulative braking energy dissipated by the braking system for the whole endurance campaign. As expected, the obtained measurements show an overall decreasing tendency of the braking friction coefficient μ_b with respect to the dissipated braking energy for each subsequent maneuver. The decreasing trend exhibits a nonlinear characteristic, with a fast initial degradation regime followed by a slow decreasing deterioration zone until the worn out condition is reached. Even though the general trend of the decay is clear and repeatable, there is also a certain variability, which can be explained due to local temperature gradients on the actuator and its own nonlinear behavior, which exhibits hysteresis between successive braking experiments.

In order for a simulator to capture such an effect, probabilistic modeling tools provide a suitable balance between the fitting accuracy, and the preservation of the variability inherent in such a complex phenomenon as braking pad sliding contacts. In particular, Gaussian Mixture Models (GMM) have the capability of modelling complex multimodal probability distributions while maintaining a simple analytical description.

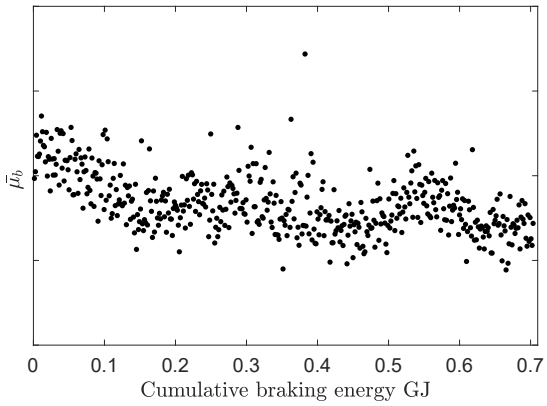

Fig. 7. Evolution of the mean braking friction coefficient against the cumulative energy dissipated by the braking pads of the test rig landing gear while performing the endurance tests of identical 500 braking maneuvers.

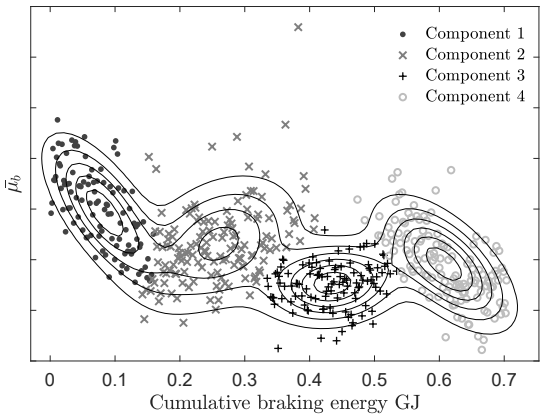

Fig. 8. Contour plot of the obtained GMM probability density function after the learning process. The data is overlaid and distinctly colored to show the membership of each data point on the most likely Gaussian component out of the four.

GMMs are a popular approach in prognosis and have been used with success in applications such as fault diagnosis and performance degradation assessment of bearings by capturing the healthy data distribution [42], construction of degradation indices in aviation piston pumps [43] and condition monitoring of machine tool wear [44]. A similar approach will be followed in this work to characterize the probability distribution of the observed endurance tests. A GMM describes a probability distribution as a weighted sum of M mixture components, each of them being a normal probability distribution with a certain weight $w_i \in (0, 1)$. The probability density $p(x|\phi)$ of the GMM will read

$$p(x|\phi) = \sum_{i=1}^{M} w_i \frac{e^{-\frac{1}{2}(x-\mu_i)^T \sigma_i^{-1}(x_i-\mu_i)}}{\sqrt{(2\pi)^k det(\sigma_i)}} \tag{10}$$

$$\sum_{i=1}^{M} w_i = 1 \tag{11}$$

where σ_i is the covariance matrix of the i-th component, μ_i is the mean vector of the i-th component, x is the vector of regressors and $\phi = [\mu_1, \sigma_1, \ldots, \mu_M, \sigma_M]$ is the vector of parameters. Due to the physical considerations related to the endurance tests, the vector of regressors was chosen to be composed by the cumulative energy absorbed by the disc brake c_e, and by the mean disc brake friction coefficient $\overline{\mu_b}$ across a braking maneuver, i.e.,

$$x = \begin{bmatrix} c_e \\ \overline{\mu_b} \end{bmatrix} \tag{12}$$

In this manner, each Gaussian component was described by a 2-dimensional normal distribution. A possibility to obtain a set of parameters ϕ^* that describe adequately the n observations is to maximize the log-likelihood function

$$\log(L(x|\phi)) = \log\Big(\prod_{i=1}^{n} p(x^i|\phi)\Big) \tag{13}$$

The common technique used to solve iteratively the problem is to use the Expectation-Maximization (EM) algorithm [45], which alternates between an Expectation step (E) in which the expectation of the log-likelihood function is computed with the current parameter estimates, and a Maximization step (M) in which the parameters are adjusted to maximize the previously computed expectation. By doing so, the EM algorithm will find local optima of the log-likelihood function. Hence, iterating the algorithm using a rich set of initial conditions contributes in obtaining a descriptive ϕ^*. In order to use the EM algorithm with the measured braking actuator data to identify the set of parameters ϕ required by the GMM in Equation (10), the amount of Gaussian mixture components M must be fixed. There are several ways to choose this parameter. In this work, the Bayesian Information Criterion (BIC) was used to discriminate between model classes of different complexity, by penalizing the amount of estimated parameters contained in each model [46]. Different model classes were generated by varying parameter M between 1 to 15, and for each model class the parameter set ϕ was identified using the measured data together with the EM algorithm. The parameter search for ϕ was initialized from 100 random initial values, keeping the set ϕ^* that maximized the log-likelihood function from Equation (13) for each of the 15 model classes explored. After the procedure, the minimum BIC was attained at a value of $M = 4$, which allowed to select its corresponding parameter set ϕ^* as the output of the optimization routine. The contour plot of the learned probability density function against the data can be appreciated in Fig. 8.

The identified data-driven distribution is useful to emulate the real-world evolution of the degradation of the braking actuator, thus completing the capabilities of the validated rigid body model presented in Section III. For every simulated maneuver, the value of the cumulative energy c_e is recorded, and the next landing maneuver will experience a mean friction coefficient of $\overline{\mu_b}$ that will depend on the identified distribution. A simple procedure to numerically extract this value is to find the closest Gaussian component j in the energy axis and resort to the conditional probability density

$$P(\overline{\mu_b}|c_e = a) \sim N\Big(\overline{\mu_b}^j + \frac{\sigma_b^j}{\sigma_{c_e}^j}\rho^j(a - \overline{\mu_{c_e}}^j), (1-\rho^2)(\sigma_b^j)^2\Big) \tag{14}$$

where ρ^j is the correlation coefficient of the j-th component,

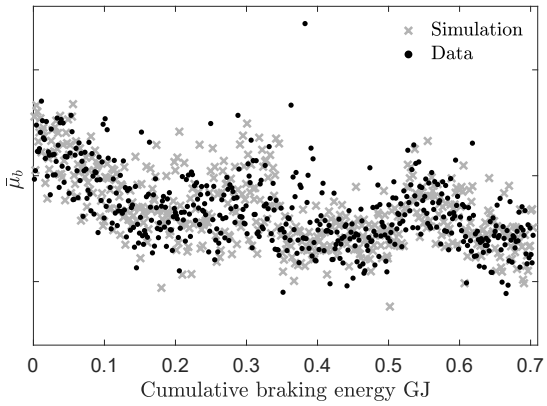

Fig. 9. Comparison between the simulation output and the recorded data points of the evolution of the mean braking friction coefficient against the cumulative energy dissipated by the braking pads. The simulator was fed the same braking torque as in the endurance tests.

σ_b^j the standard deviation of the j-th component of the braking friction, $\sigma_{c_e}^j$ the standard deviation of the j-th component of the cumulative braking energy, $\overline{\mu_b}^j$ the mean of the j-th component of the braking friction and $\overline{\mu_{c_e}}^j$ the mean of the j-th component of the cumulative braking energy. Once the conditional probability density is obtained, a random value $\overline{\mu_b}$ is drawn and the mean braking friction coefficient for the next landing maneuver can be identified. An example of the results obtained with this procedure can be appreciated in Fig. 9, in which the 500 landing maneuvers were replicated in the simulator by feeding the braking torque measured in the endurance tests, while the mean friction coefficient $\overline{\mu_b}$ is computed with the simulator. The dynamic evolution of μ_b was described by a suitably biased version of the Light Landing curve, adapted to match the extracted mean. A remarkable match is appreciated between the trend of recorded observations and the simulated ones, demonstrating the capabilities of the augmented simulator in capturing the braking actuator degradation phenomenon by using the cumulative absorbed braking energy.

V. The wheel slip-based anti-skid controller

In order to analyse how the braking actuator usage status and the tire energy consumption can be directly related to the anti-skid controller parameters, a wheel slip anti-lock braking system was designed and an analysis was performed on how the energy distribution for these two components depends on the wheel slip set-point value $\bar{\lambda}$, selected for the controller tracking performance. The slip controller was selected due to the straightforward tuning procedure and the possibility to extract a direct relationship between its parameters and component wear, already proved in [22], [23]. A simplified schematic representation of the controller is represented in Fig. 10. In the control scheme represented in Fig. 10, the controller receives as input the wheel slip error, computed as the difference between the reference wheel slip value and the measured one, that is $\bar{\lambda} - \lambda$, and provides as output the current reference value, which is converted into the braking torque T_b by the actuator, and applied on the landing gear.

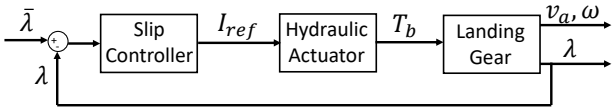

Fig. 10. Block diagram representation of the wheel slip controller.

Within this framework, the anti-lock braking system can be formulated as a wheel slip tracking task, with the control law being defined by solving a continuous dynamic problem, see again [1], [3], [11]. With reference to the control scheme in Fig. 10, the wheel slip controller is designed on the transfer function $L(s)$ given by $L(s) = G_\lambda(s) \cdot A(s)$, with $A(s)$ being the actuator transfer function described in Equation (6), and $G_\lambda(s)$ the linearized transfer function between the braking torque T_b and the wheel slip λ computed at the equilibrium point $\bar{\lambda}$. The wheel slip estimator dynamic will not be included in the controller design, as the wheel slip will be assumed to be measurable for the control problem at hand, being the estimation problem outside the scope of the present work. The analytical expression for the linearized torque to wheel slip transfer function can be derived starting from the dynamical model in equation (1b), and considering standard assumptions from the automotive literature, *i.e.* slowly varying longitudinal velocity $\bar{v}_a$, that is

$$G_\lambda(s) = \left(\frac{r}{J\bar{v}_a}\right)\left(\frac{1}{s + \frac{F_z}{m\bar{v}_a}\mu_1(\bar{\lambda})\left((1-\bar{\lambda}) + \frac{mr^2}{J}\right)}\right) \quad (15)$$

where $\mu_1(\bar{\lambda})$ is defined as the slope of the $\mu(\lambda)$ curve at the equilibrium point $\bar{\lambda}$. The controller must be designed so as to be robust with respect to different aircraft operating conditions. Within this work of research we identified four possible mass configurations of interest, and eight friction cases spanning from dry asphalt to snow, and by combining them we defined a matrix of 32 different operating conditions. The transfer function $L(s)$ has been computed for each considered case, and its spread can be appreciated in Fig. 11. A Proportional Integral Derivative (PID) structure has been selected for the wheel slip controller, and its parameters tuned so as to guarantee the required performance: phase margin $PM \geq 30$ deg and gain margin $GM \geq 30$ dB for the whole spectrum of loop transfer functions.

Fig. 12 shows the velocity, pressure and wheel slip profiles for a simulated heavy dry-landing braking maneuver, with the scale omitted for confidentiality reasons. Comparing the resulting wheel slip profile to that of the requested set-point $\bar{\lambda}$, it is clear that the defined wheel slip controller allows an accurate tracking of the considered reference $\bar{\lambda}$ over the whole maneuver, with some oscillations possibly linked to the activation phase.

VI. Braking actuator and tire - wear energy sensitivity analysis

The relation between the braking actuator and tire energy consumption with the key design parameter of the defined

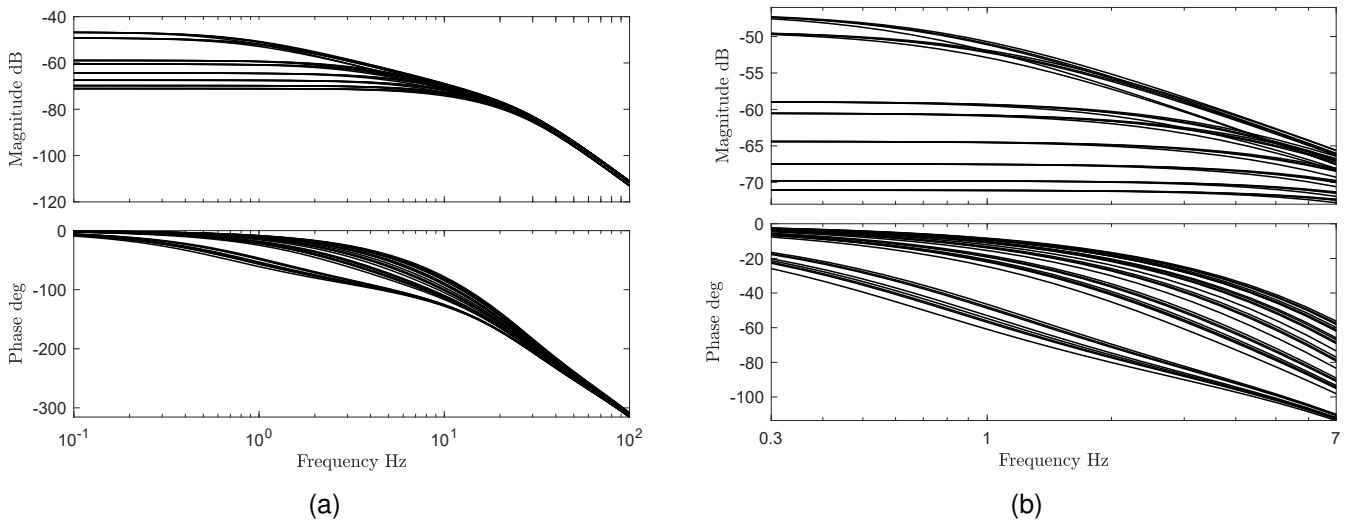

Fig. 11. Transfer function $L(s)$ over the 32 scenarios considered. Each of the four standard landing maneuver types are analyzed in the eight different runway friction conditions. (a): Overview of the transfer function spread. (b): Local enlargement around the relevant frequency range of the control system.

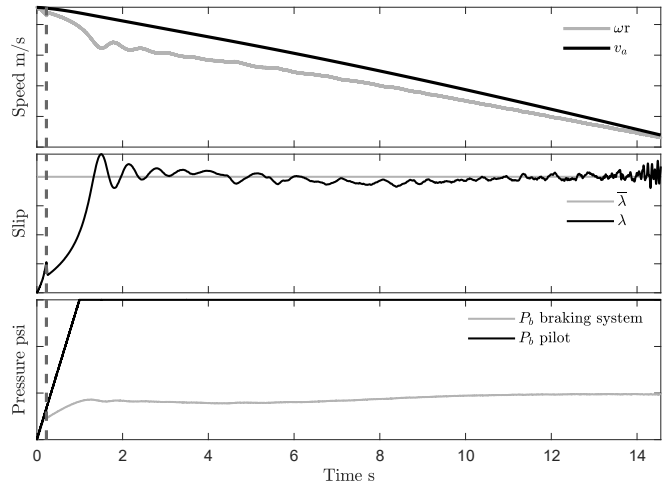

Fig. 12. Closed loop behavior of the wheel slip control system on a Heavy Landing maneuver. Top plot: Time histories of aircraft and wheel speeds. Middle plot: Time histories of the reference and obtained wheel slip. Bottom plot: Time histories of the pressure requested by the pilot and pressure actually applied by the control system. The vertical dotted line indicates the instant when the controller engages.

wheel slip based anti-skid controller has been studied from a set of multiple closed loop maneuvers with varying reference wheel slip value. The braking maneuvers are carried out in a very wide array of working conditions using the simulation environment described in Section III, coupled with the braking actuator wear dynamic described in Section IV. First, a set of 32 possible scenarios comprising of different tire-road friction conditions, and pairs of different aircraft masses and initial speed values, were defined. The 32 different scenarios are obtained by combining the 8 friction curves, see Fig. 3, with the different 4 aircraft configurations reported in Table II. Then, a set of 100 maneuvers were randomly chosen among the pool of 32 scenarios. The anti-skid controller has been evaluated on the set of 100 maneuvers with a fixed wheel slip reference value in each of them. Different wheel slip reference values have been tested ranging from $\bar{\lambda} = 0.06$ to $\bar{\lambda} = 0.5$ for a total of 45, thus covering both the stable and unstable regimes for all friction conditions, see again Fig. 3. The overall data set consists of 45 sets of maneuvers, each of these containing 100 closed loop braking maneuvers performed with a single wheel slip reference value, for a total of 4500 maneuvers. For each tested reference wheel slip value, two relevant statistics, directly connected to the anti-skid performance, are computed over the set of 100 maneuvers: the braking distance, which is the most widely used performance indicator for braking controllers, and the capability of the braking control system to exploit the available road-friction. For the latter, the following cost function J_μ is used

$$J_\mu = \frac{\int_{t_{\text{start}}}^{t_{\text{end}}} \mu(t) dS(t)}{\int_{t_{\text{start}}}^{t_{\text{end}}} \mu_{\max}(t) dS(t)} \tag{16}$$

where t_{start} and t_{end} represent the start and the end of the braking maneuver, respectively, $\mu_{\max}$ is the maximum available friction characteristic of the runaway and $dS(t)$ is the infinitesimal space displacement. This cost function has a direct physical meaning: ideally $J_\mu = 1$ can be reached if the maximum available friction is exploited during the whole braking maneuver. High performing braking controllers ensure that J_μ is in the interval $[0.85 - 1.00]$ in all the tested conditions.

The results from the sensitivity analysis are compactly reported in Fig. 13, which shows the mean of the two considered performance indexes, *i.e.* J_μ and braking distance d, against the average value of the consumed energy over each set of 100 maneuvers, for different wheel slip reference values $\bar{\lambda}$. The following conclusions can be derived from Fig. 13. In the first place, note that the trends in the two cost functions for both the braking actuator and tire, exhibit the same behavior. For low wheel-slip reference values, which corresponds to slowly decelerating maneuvers, the braking

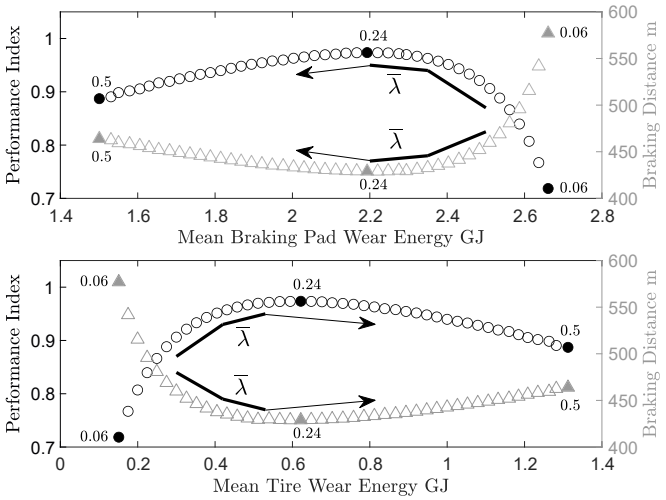

Fig. 13. Results of the sensitivity analysis of mean performance index J_μ and required braking distance to anti-skid control slip reference. Top: Performance quantities as a function of the dissipated braking pad energy. Bottom: Performance quantities as a function of the dissipated tire wear energy. The arrow points towards an increasing value of the slip reference, between 0.06 and 0.5 units.

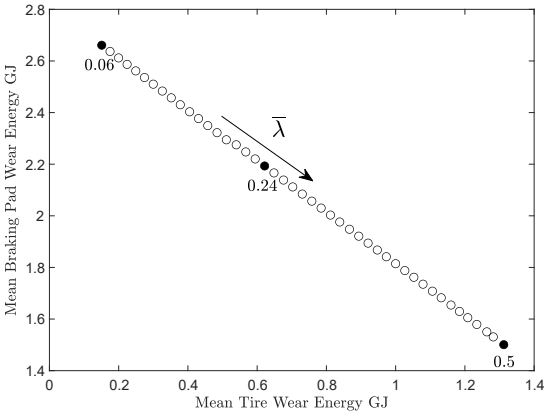

Fig. 14. Results of the sensitivity analysis of braking pad and tire wear dissipated energy to anti-skid control slip reference. The arrow points towards an increasing value of the slip reference, between 0.06 and 0.5 units.

distance d increases while J_μ decreases. The opposite trend is observed for high wheel-slip reference values, with the only difference being the steepness of the trend: much higher for low slip values. This feature can be explained by considering the employed friction curve $\mu(\lambda)$, which shows the same trend when moving leftwards by decreasing λ, or rightwards by increasing λ starting from its peak value. Secondly, it is observed from the two graphs that, regardless of the wheel slip reference value $\bar{\lambda}$, the mean energy consumed by the braking system is much higher than that consumed by the tire. Furthermore, the two cost functions exhibit a complementary tendency with respect to the mean consumed energy for the two components. In fact, the total mechanical energy of the aircraft for the considered case is dissipated via these two components. The more the energy consumed by the braking actuator, the less that absorbed by the tire. With this braking control strategy, the wheel slip reference value $\bar{\lambda}$ determines the energy distribution between these two components: high reference values correlate to higher tire wheel consumption, while low ones correspond to high braking pad consumption. By considering the expression of the braking energy provided in equation (9), if the wheel slip is equal to one (wheel locking condition) for the whole braking maneuver, then the value of $\omega(t)$ is equal to zero, resulting in a null contribution of the energy component associated to the braking actuator and leaving all the energy dissipation to the tire.

This correlation is highlighted in Fig. 14, which compares the energy consumed by the two components for different wheel-slip values. The same trend repeats here, as in fact for higher wheel slip reference values the energy consumption shifts from the braking actuator to the tire. Combining Fig. 13 and Fig. 14 a trade-off for the consumption of the two components can be found, and this corresponds to a wheel slip reference value of $\bar{\lambda} = 0.24$. When selecting this value for the wheel-slip reference, the anti-skid controller not only guarantees limited consumption in both components but also allows for performance maximization reaching an average performance index value of $J_\mu = 0.97$ for the whole dataset of 100 maneuvers. These results show that by framing the braking control problem as a wheel slip regulation one, it is possible to have a direct control on braking actuator and tire energy consumption, and on the mix between the two. Also, by properly selecting the controller parameters, *i.e.* the wheel slip reference value, maximum braking performance can be reached while maintaining limited consumption for both components. This result is significant, as it shows that the braking problem can be formulated as the regulation of brake and tire usage while ensuring safety and performance in the braking maneuvers, offering the way to balance the different goals and have an effective means for predictive maintenance goals thanks to the possibility of monitoring the brake degradation along the aircraft life and usage history.

VII. Concluding remarks

This paper analysed the relation between the anti-skid controller parameters and the braking actuator and tire energy consumption. The analysis is carried out in a Matlab Simulink simulation environment, where a rigid body model, validated experimentally, for a single Main Landing Gear has been implemented, coupling all the relevant dynamics and including a detailed model for the braking actuator which considers the wear dynamic of the component over its lifespan, as measured from real experimental data. A wheel-slip based anti-skid controller has been designed to investigate the relation between the consumed energy in both components (tire and brake) and the controller set-point value. In order to do this, an initial set of 100 different maneuvers was defined, comprising multiple aircraft operating conditions in terms of mass, road friction and initial velocity. Then, closed-loop experiments with varying reference wheel-slip values for a total of 4500 braking maneuvers were performed. The tire and braking actuator consumed energy along with braking performance statistics were extracted from this dataset and their values compared. The results not only demonstrate the existence of a direct relation between wheel slip reference value and the

energy consumption for the two components, but they also show that by properly selecting this value, limited tire and braking actuator usage can be achieved while maximizing the braking performance. These relevant results open the way to combined control of braking maneuvers while regulating also the wear of brakes and tires.

REFERENCES

[1] T. A. Johansen, I. Petersen, J. Kalkkuhl, and J. Ludemann, "Gain-scheduled wheel slip control in automotive brake systems," *IEEE Transactions on Control Systems Technology*, vol. 11, no. 6, pp. 799–811, 2003.

[2] M. Tanelli, A. Astolfi, and S. M. Savaresi, "Robust nonlinear output feedback control for brake-by-wire control systems." *Automatica*, vol. 44, no. 4, pp. 1078–1087, 2008.

[3] M. Corno, S. S.M., and G. Balas, "On linear parameter varying (lpv) slip-controller design for two-wheeled vehicles," *International Journal of Robust and Nonlinear Control*, vol. 19, no. 12, pp. 1313–1336, 8 2009.

[4] K. R. Buckholtz, "Reference input wheel slip tracking using sliding mode control," *Sae Transactions*, pp. 477–483, 2002.

[5] D. Savitski, D. Schleinin, V. Ivanov, and K. Augsburg, "Robust continuous wheel slip control with reference adaptation: Application to the brake system with decoupled architecture," *IEEE Transactions on Industrial Informatics*, vol. 14, no. 9, pp. 4212–4223, 2018.

[6] H. Jing, Z. Liu, and H. Chen, "A switched control strategy for antilock braking system with on/off valves," *IEEE Transactions on Vehicular Technology*, vol. 60, no. 4, pp. 1470–1484, 2011.

[7] R. Johansson and A. Rantzer, *Nonlinear and hybrid systems in automotive control*. Springer, 2003, ISBN 978-0-7680-1137-1.

[8] C.-M. Lin and C.-F. Hsu, "Neural-network hybrid control for antilock braking systems," *IEEE Transactions on Neural Networks*, vol. 14, no. 2, pp. 351–359, 2003.

[9] C. Kuo and E. Yeh, "A four-phase control scheme of an anti-skid brake system for all road conditions," *Proceedings of the Institution of Mechanical Engineers, Part D: Journal of Automobile Engineering*, vol. 206, no. 4, pp. 275–283, 1992.

[10] M. Tanelli, G. Osorio, M. di Bernardo, S. M. Savaresi, and A. Astolfi, "Limit cycles analysis in hybrid anti-lock braking systems," in *2007 46th IEEE Conference on Decision and Control*. IEEE, 2007, pp. 3865–3870.

[11] S. Savaresi and M. Tanelli, *Active Braking Control Systems Design for Vehicles*. London, UK: Springer-Verlag, 2010, ISBN 978-1-84996-350-3.

[12] Robert Bosch GmbH, *Automotive Handbook, 7th Edition*. Wiley, New York, 2008, ISBN10: 0837615402.

[13] M. Tanelli, G. Osorio, M. di Bernardo, S. M. Savaresi, and A. Astolfi, "Existence, stability and robustness analysis of limit cycles in hybrid anti-lock braking systems," *International Journal of Control*, vol. 82, pp. 659–678, 2009.

[14] K. Kobayashi, K. C. Cheok, and K. Watanabe, "Estimation of absolute vehicle speed using fuzzy logic rule-based kalman filter," in *Proceedings of 1995 American Control Conference-ACC'95*, vol. 5. IEEE, 1995, pp. 3086–3090.

[15] S. Semmler, D. Fischer, R. Isermann, R. Schwarz, and P. Rieth, "Estimation of vehicle velocity using brake-by-wire actuators," *IFAC Proceedings Volumes*, vol. 35, no. 1, pp. 169–174, 2002.

[16] L. R. Ray, "Nonlinear tire force estimation and road friction identification: Simulation and experiments," *Automatica*, vol. 33, no. 10, p. 1819–1833, 1997.

[17] G. Panzani, M. Corno, and S. Savaresi, "Longitudinal velocity estimation in single-track vehicles," *IFAC Proceedings Volumes*, vol. 45, no. 16, pp. 1701–1706, 2012.

[18] L. Alvarez, J. Yi, R. Horowitz, and L. Olmos, "Adaptive emergency braking control with observer-based dynamic tire/road friction model and underestimation of friction coefficient," *IFAC Proceedings Volumes*, vol. 35, no. 1, pp. 211–216, 2002, 15th IFAC World Congress.

[19] J. Yi, L. Alvarez, X. Claeys, and R. Horowitz, "Emergency braking control with an observer-based dynamic tire/road friction model and wheel angular velocity measurement," *Vehicle system dynamics*, vol. 39, no. 2, pp. 81–97, 2003.

[20] S. Rajendran, S. K. Spurgeon, G. Tsampardoukas, and R. Hampson, "Estimation of road frictional force and wheel slip for effective antilock braking system (abs) control," *International Journal of Robust and Nonlinear Control*, vol. 29, no. 3, pp. 736–765, 2019.

[21] M. Tanelli, L. Piroddi, and S. M. Savaresi, "Real-time identification of tire-road friction conditions," *IET Control Theory & Applications*, vol. 3, pp. 891–906, 2009.

[22] L. D'Avico, M. Tanelli, and S. Savaresi, "Combining tire-wear and braking control for aeronautical applications," in *2019 18th European Control Conference (ECC)*, 2019, pp. 131–136.

[23] M. Q. Chen, W. S. Liu, Y. Z. Ma, J. Wang, F. R. Xu, and Y. J. Wang, "Mixed slip-deceleration pid control of aircraft wheel braking system," *IFAC-PapersOnLine*, vol. 51, no. 4, pp. 160–165, 2018, 3rd IFAC Conference on Advances in Proportional-Integral-Derivative Control PID 2018.

[24] L. D'Avico, M. Tanelli, S. Savaresi, M. Airoldi, and G. Rapicano, "An anti-skid braking system for aircraft via mixed-slip-deceleration control and sliding mode observer," in *2017 IEEE 56th Annual Conference on Decision and Control (CDC)*, 2017, pp. 4503–4508.

[25] G. Papa, M. Tanelli, G. Panzani, and S. M. Savaresi, "A comparison of model-based and black-box methods for speed estimation in aircraft," *IFAC-PapersOnLine*, vol. 53, no. 2, pp. 14 775–14 780, 2020, 21th IFAC World Congress.

[26] S. Yu, J. Chen, Q. Huang, X. Xiong, T. Chang, and Y. Li, "Effect of braking speeds on the tribological properties of carbon/carbon composites," *Materials Transactions*, vol. 51, no. 5, pp. 1038–1043, 2010.

[27] T. Peng, Q. Yan, G. Li, X. Zhang, Z. Wen, and X. Jin, "The braking behaviors of cu-based metallic brake pad for high-speed train under different initial braking speed," *Tribology Letters*, vol. 65, no. 4, pp. 1–13, 2017.

[28] S. Fan, L. Zhang, L. Cheng, G. Tian, and S. Yang, "Effect of braking pressure and braking speed on the tribological properties of c/sic aircraft brake materials," *Composites Science and Technology*, vol. 70, no. 6, pp. 959–965, 2010.

[29] F. Braghin, F. Cheli, S. Melzi, and F. Resta, "Tyre wear model: validation and sensitivity analysis," *Meccanica*, vol. 41, no. 2, pp. 143–156, 2006.

[30] Y. Li, S. Zuo, L. Lei, X. Yang, and X. Wu, "Analysis of impact factors of tire wear," *Journal of Vibration and Control*, vol. 18, no. 6, pp. 833–840, 2012.

[31] J. F. Archard, "Contact and rubbing of flat surfaces," *Journal of Applied Physics*, vol. 24, no. 8, pp. 981–988, 1953.

[32] A. R. AbuBakar and H. Ouyang, "Wear prediction of friction material and brake squeal using the finite element method," *Wear*, vol. 264, no. 11, pp. 1069–1076, 2008.

[33] P. C. Verma, L. Menapace, A. Bonfanti, R. Ciudin, S. Gialanella, and G. Straffelini, "Braking pad-disc system: Wear mechanisms and formation of wear fragments," *Wear*, vol. 322-323, pp. 251–258, 2015.

[34] L. D'Avico, M. Tanelli, and S. Savaresi, "Experimental validation of landing-gear dynamics for anti-skid control design," in *2018 European Control Conference (ECC)*, 2018, pp. 2751–2756.

[35] W. Krüger and M. Morandi, "Numerical simulation of landing gear dynamics: State-of-the-art and recent developments," in *AVT-152 Symposium on Limit Cycle Oscillation and Other Amplitude-Limited Self-Excited Vibrations*, 2008.

[36] S. Gualdi, M. Morandini, and G. L. Ghiringhelli, "Anti-skid induced aircraft landing gear instability," *Aerospace Science and Technology*, vol. 12, no. 8, pp. 627–637, 2008.

[37] M. Rahmani and K. Behdinan, "Investigation on the effect of coulomb friction on nose landing gear shimmy," *Journal of Vibration and Control*, vol. 25, no. 2, pp. 255–272, 2019.

[38] P. E. Evans, "Modeling and simulation of tricycle landing gear at normal and abnormal conditions," Master's thesis, College of Engineering and Mineral Resources at West Virginia University, 2010, graduate Theses, Dissertations, and Problem Reports. 2153.

[39] G. Ostermeyer, "On the dynamics of the friction coefficient," *Wear*, vol. 254, no. 9, pp. 852–858, 2003, 280th We-Hereaus Seminar Integrating Friction and Wear Research.

[40] V. Ricciardi, A. Travagliati, V. Schreiber, M. Klomp, V. Ivanov, K. Augsburg, and C. Faria, "A novel semi-empirical dynamic brake model for automotive applications," *Tribology International*, vol. 146, p. 106223, 2020.

[41] S. Andersson, "Wear simulation," in *Advanced Knowledge Application in Practice*, I. Fuerstner, Ed. Rijeka: IntechOpen, 2010, ch. 2, pp. 15–37.

[42] J. Yu, "Bearing performance degradation assessment using locality preserving projections and gaussian mixture models," *Mechanical Systems and Signal Processing*, vol. 25, no. 7, pp. 2573–2588, 2011.

[43] C. Lu and S. Wang, "Performance degradation prediction based on a gaussian mixture model and optimized support vector regression for an aviation piston pump," *Sensors*, vol. 20, no. 14, 2020.

[44] J. Yu, "Machine Tool Condition Monitoring Based on an Adaptive Gaussian Mixture Model," *Journal of Manufacturing Science and Engineering*, vol. 134, no. 3, 2012.

[45] A. P. Dempster, N. M. Laird, and D. B. Rubin, "Maximum likelihood from incomplete data via the em algorithm," *Journal of the Royal Statistical Society: Series B (Methodological)*, vol. 39, no. 1, pp. 1–22, 1977.

[46] G. Schwarz, "Estimating the dimension of a model," *The Annals of Statistics*, vol. 6, no. 2, pp. 461–464, 1978.